DOI: 10.1002/adma.200501953

Crystalline WO_3 Nanoparticles for Highly Improved Electrochromic Applications**

By *Se-Hee Lee*, *Rohit Deshpande*, *Phil A. Parilla*, *Kim M. Jones*, *Bobby To*, *A. Harv Mahan*, and *Anne C. Dillon**

Electrochromic (EC) materials change their optical properties (darken/lighten) in the presence of a small electric potential difference, and are suitable for application in energy-efficient windows, antiglare automobile rear-view mirrors, sunroofs, displays, and hydrogen sensors.[1–4] The operation of conventional EC devices depends on the reversible electrochemical double injection of positive ions (H^+, Li^+, Na^+) and electrons into the host lattice of multivalent transition metal oxide materials,[5–10] with positive-ion insertion required to satisfy charge neutrality. However, diffusion of positive ions into the oxide layer is often slow, taking minutes to complete. Since the chemical diffusion coefficient of protons (D_{H^+}) is an order of magnitude larger than that of lithium ions (D_{Li^+}), EC systems based on proton electrolytes (e.g., aqueous H_2SO_4) are mandatory for display applications and preferred for other applications. Unfortunately, proton insertion currently results in rapid degradation of EC films.

There are two important criteria for selecting an EC material. The first is the time constant of the ion-intercalation reaction, which is limited both by the diffusion coefficient and by the length of the diffusion path. While the former depends on the chemical structure and crystal structure of the metal oxide, the latter is determined by the material's microstructure.[11] In the case of a nanoparticle, the smallest dimension is represented by the diffusion path length. Thus, designing a nanostructure with a small radius, while maintaining the proper crystal structure, is key to obtaining a material with fast insertion kinetics, enhanced durability, and superior performance. The second important criterion is coloration efficiency (CE), the change in optical density (OD) per unit inserted charge (Q), that is, $CE = \Delta(OD)/\Delta Q$.[12] A high CE provides large optical modulation with a small charge insertion or extraction. This is a crucial parameter for EC devices, since a lower charge-insertion or -extraction rate enhances the long-term cycling stability. Among inorganic materials, tungsten oxides have been most extensively studied. Up until now, amorphous WO_3 films have exhibited the highest CE in the visible region of the electromagnetic spectrum. However, because of their high dissolution rate in acidic electrolyte solutions, these films can only be used in lithium-based electrolytes, resulting in slower response times. Furthermore, extended durability, even in Li^+ systems, has not yet been demonstrated. Inexpensive conducting and redox polymers have attracted increased attention for use as EC materials because of their fast response times and high contrast ratios.[13–15] However, disadvantages include multiple coloration in the visible spectral range and poor UV stability.

By fabricating EC films from crystalline WO_3 nanoparticles, the state-of-the-art technology of producing EC materials has been profoundly advanced. Crystalline WO_3 nanoparticles have been grown by an economical hot-wire chemical-vapor-deposition (HWCVD) process, and a unique electrophoresis technique is employed for the fabrication of porous nanoparticle films. The porosity of the films not only increases the surface area and ion-insertion kinetics, but also reduces the overall material cost, leading to an inexpensive, large-area EC material. Compared to conventional amorphous WO_3 films prepared by vacuum deposition, nanoparticle films deposited by electrophoresis exhibit vastly superior electrochemical-cycling stability in acidic electrolytes, a higher charge density, and comparable CE. This greatly enhanced stability and charge capacity are attributed to the crystalline nanoparticles employed in this work. These initial results will ultimately revolutionize all EC applications. Furthermore, preliminary results show that these advances will impact developing battery technologies.

Thin films of WO_3 nanoparticles were deposited by a unique electrophoresis deposition process (EDP) on SnO_2:F-coated glass substrates. Although the EDP-deposited WO_3 nanoparticle films were blue, indicating a substoichiometric composition of tungsten oxide nanoparticles, they became transparent after annealing in air at 300 °C for 2 h. Figure 1 displays the X-ray diffraction (XRD) spectra of the as-synthesized nanoparticle-containing powder, an EDP-deposited film, an annealed EDP-deposited film, and the substrate. All of the spectra of the tungsten oxide nanoparticles have crystalline features consistent with WO_3 crystals of both the monoclinic (I) γ-phase and the monoclinic (II) ε-phase. Furthermore, the as-synthesized nanoparticle-containing pow-

[*] Dr. A. C. Dillon, Dr. S.-H. Lee, R. Deshpande, Dr. P. A. Parilla, K. M. Jones, B. To, Dr. A. H. Mahan
National Renewable Energy Laboratory
1617 Cole Blvd., Golden, CO 80401 (USA)
E-mail: anne_dillon@nrel.gov
Dr. A. C. Dillon
Division of Basic Sciences
National Renewable Energy Laboratory
1617 Cole Blvd., Golden, CO 80401 (USA)

[**] This work was funded by the U.S. Department of Energy Director's Discretionary Research and Development Funding under subcontract DE-AC36-99GO10337 to NREL.

ADVANCED MATERIALS

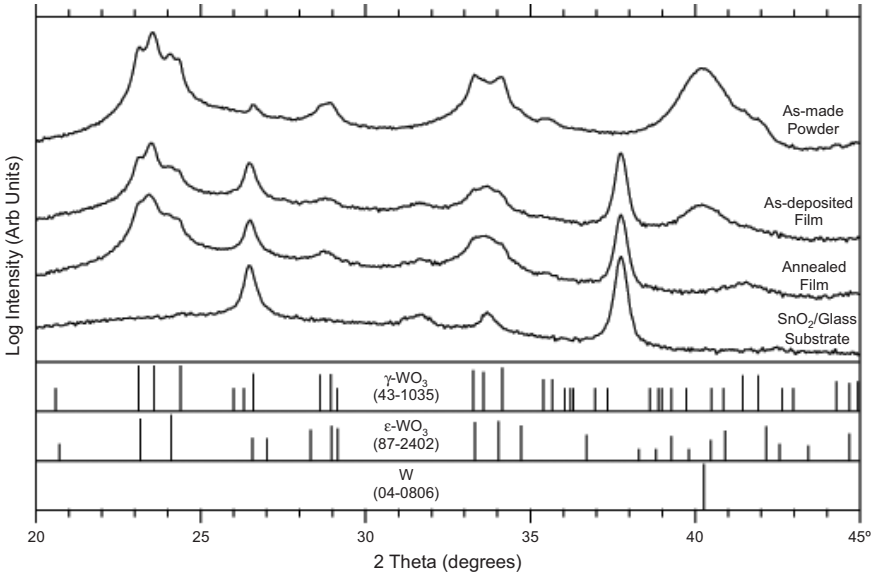

Figure 1. XRD spectra of the as-synthesized nanoparticle-containing powders, the EDP-deposited film, the annealed EDP-deposited film, and the blank SnO_2:F-coated glass substrate. In order to make relative comparisons, all spectra of the oxide nanoparticle materials were normalized to the strongest line appearing for the monoclinic (I) γ-phase.

der and, to a lesser extent, the EDP-deposited film, display a line indicating the presence of tungsten metal. It is interesting to note that the EDP reduces the metal content, so the film has less tungsten metal than the as-synthesized powder (the presence of metal would negatively affect the EC properties of the film.) The remainder of the metal is easily removed by brief oxidative annealing.

Figure 2a shows a representative transmission electron microscopy (TEM) image of the tungsten oxide nanoparticles employed in our study. The nanoparticles consist predominantly of nanorods and nanospheroids. The nanospheroids have diameters between approximately 10 and 20 nm and the nanorods have similar diameters with lengths of approximately 40 to 60 nm. Figure 2b displays a scanning electron microscopy (SEM) image of an EDP-deposited film. It is clearly evident that these films are highly porous with large active surface areas, and the nanoparticle size is unchanged. As corroborated by cyclic voltammetry measurements, this large surface area results in very significant improvements in the EC properties. Consistent with the SEM studies, the mass density of the nanoparticle film has been found to be approximately 2.5 $g\,cm^{-3}$, estimated from mass and thickness data. Since the theoretical bulk density of monoclinic WO_3 is 7.2 $g\,cm^{-3}$, the pore volume of the nanoparticle films was calculated to be 0.26 $cm^3\,g^{-1}$, which is comparable to values of mesoporous metal oxides.[16] Figure 2c displays a TEM image of nanoparticles deposited at a lower synthesis pressure. WO_3 nanoparticles composed of only nanospheroids with a monoclinic crystalline structure coated with an amorphous overlayer were obtained. Interestingly, thin films of these particles deposited by the same EDP exhibit inferior EC properties.

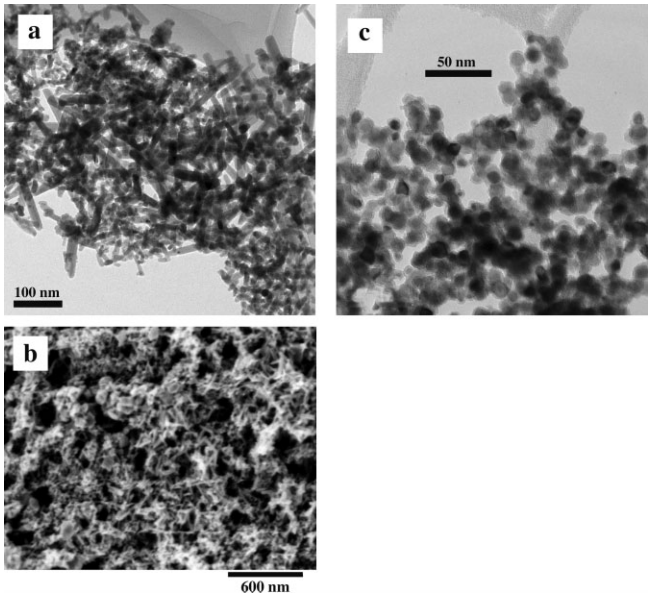

Figure 2. a) TEM image of HWCVD-generated WO_3 nanoparticles (nanorods and nanospheroids). b) Scanning electron microscopy (SEM) image of the WO_3 films deposited by electrophoresis. c) TEM image of nanoparticles deposited at a lower working pressure.

Figure 3a compares the cyclic voltammograms (CVs), measured in 1 M H_2SO_4, of an optimal tungsten oxide nanoparticle film (Fig. 2b), a conventional amorphous film, and a crystalline film. All of the CVs were normalized to the geometric area of the electrode and to the weight of tungsten oxide within that area, resulting in units of $mA\,cm^{-2}\,mg^{-1}$. In general, when the tungsten oxide films were cathodically polarized in H_2SO_4, they had a very uniform blue color, which intensified with increasing cathodic potential. When the blue films were anodically polarized, they were bleached and transparent. The integrated cathodic-current density equates to the amount of protons intercalated to form a tungsten bronze. When compared with the cathodic charge quantities of amorphous and crystalline tungsten oxide films, the nanoparticle films show a higher charge-insertion density over the same time period, indicating faster kinetics. The total cathodic

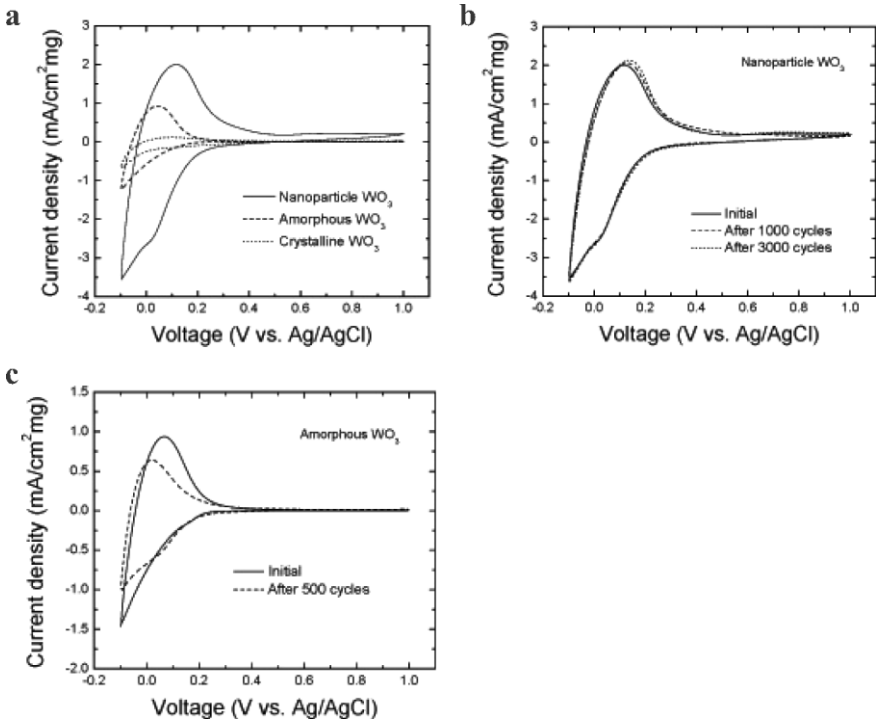

Figure 3. a) CVs of the WO_3 films deposited by electrophoresis of WO_3 nanoparticles, by thermal evaporation (amorphous), and by thermal evaporation followed by annealing at 400 °C for 2 h (crystalline). b) CVs of a WO_3 nanoparticle film after a single cycle and after 1000 and 3000 cycles. c) CVs of an amorphous WO_3 film after a single cycle and after 500 cycles. All CVs were measured in 1 M H_2SO_4 with a sweep rate of 20 mV s^{-1}.

charge for the WO_3 nanoparticles was about 32 mC cm^{-2} mg^{-1}, compared to only about 3 mC cm^{-2} mg^{-1} for crystalline and about 9 mC cm^{-2} mg^{-1} for amorphous films—translating to a greater EC efficiency. The improved hydrogen-insertion ability of the nanoparticle film is attributed to its low density (2.5 g cm^{-3}) and high active surface area, compared with amorphous and crystalline films (5.5 and 6.4 g cm^{-3}, respectively).[17] Note also that the onset of a cathodic current for the nanoparticle electrode is more positive compared with crystalline and amorphous films. This early onset of a cathodic current for nanoparticle films may indicate reduced interfacial charge-transfer resistance, providing another reason for the improved electrochemical response.

The cycling stability of WO_3 nanoparticle films was examined in 1 M H_2SO_4 (Fig. 3b). It can be seen that the current response increases slightly during the course of 3000 cycles, without a significant change in the shape of the CVs, indicating excellent cycling stability of the nanoparticle films even in an acidic solution. A similar stability for amorphous tungsten oxide-based EC films in an acidic environment has never been achieved.[18,19] To confirm this result, the cycling stability of an amorphous WO_3 film was also examined in 1 M H_2SO_4 and the result is shown in Figure 3c. As can be seen, the amorphous WO_3 film degrades significantly after only 500 cycles in the acidic electrolyte. In a recent report, large nanoparticles of WO_3 with diameters ranging from 45 to 330 nm were employed; however, no cycling-stability experiments were reported.[20]

As stated previously, one of the most important criteria for selecting an EC material is its CE.[12] A high CE can provide large optical modulation with small changes in insertion or extraction quantities, and is a crucial parameter for practical devices, because long-term cycling stability is enhanced by using lower charge insertion or extraction. It has been reported that the CE of WO_3 films is influenced by the deposition conditions and is intimately related to oxygen deficiency.[21,22] Thus, the CE of our WO_3 nanoparticle films was measured by using a constant discharge current. Figure 4 shows a plot of in situ OD versus time. From the slope of these curves, the CE can be calculated. The CE of optimized crystalline nanoparticle films was measured to be about 42 cm^2 C^{-1}, which is comparable to amorphous WO_3 films (55 cm^2 C^{-1}).[6,12] The slight decrease in CE compared to state-of-the-art amorphous films could be compensated for by slightly increasing the potential used in the cyclic voltammetry measurements, to a potential at which the crystalline nanoparticle films are still expected to be durable.

For comparison, Figure 4 also shows a plot of in situ OD versus time for nanoparticle films prepared by the EDP and deposited at a lower synthesis temperature (Fig. 2c). Here, the CE is only 24 cm^2 C^{-1}, significantly less than that of the optimized nanoparticle films. It is interesting to consider why the optimized nanoparticles displayed in Figure 2a have a bet-

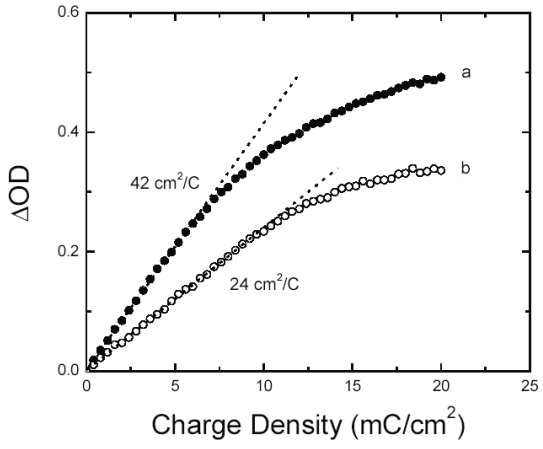

Figure 4. Variation of in situ OD in WO_3 nanoparticle thin films: a mixture of nanorods and nanospheroids (a), and only nanospheroids (b). The OD was measured at 670 nm and at a discharge-current density of 10 μA cm^{-2}.

ADVANCED MATERIALS

ter CE than those displayed in Figure 2c. One immediate observation is that the nanoparticles shown in Figure 2c are, in general, two times larger in diameter, leading to a smaller surface area than in the optimized nanoparticle film. Previous reports have shown a decrease of CE as amorphous WO_3 films crystallize into large particles during the annealing procedure.[23,24] Also, when the synthesis pressure is reduced, no nanorods are observed in the as-deposited materials. Thus, the optimal EC properties of the WO_3 nanoparticle films in Figure 2b could simply be attributed to particle size or possibly to the presence of nanorod-shaped structures.

In summary, crystalline nanoparticles consisting of nanorods and nanospheroids have been successfully fabricated by a cost-effective HWCVD process. Thin films of crystalline tungsten oxide nanoparticles have been deposited by electrophoresis on substrates suitable for large-area EC applications. Compared with conventional amorphous WO_3 films, the crystalline WO_3 nanoparticle films show greater charge density for proton intercalation and comparable CE. The improvements in the EC properties of these nanoparticle thin films have been attributed to a larger active surface area and to the low density of the films. The nanoparticle films exhibit excellent cycling stability in 1 M H_2SO_4, with values greatly surpassing those for amorphous WO_3 films. These nanoparticle oxide materials have improved response times because of their stability towards proton insertion when compared to conventional EC electrode materials. These results will significantly impact current EC technologies and have promising implications for the development of novel batteries.

Experimental

The HWCVD synthesis of nanostructured materials has been described previously by Mahan et al. and Dillon et al. [25,26]. For EC applications, the process was optimized in argon at 50 Torr (1 Torr = 133 Pa) containing a partial pressure of about 16 % oxygen at 300 °C. A single W filament (0.5 mm in diameter, 20 cm in length) was resistively heated to 1400 °C. A typical deposition was about 15 min in duration. A unique EDP technique was used to deposit thin films of WO_3 nanoparticles on SnO_2:F-coated glass substrates. In the EDP process, a nanocrystalline particle suspension was made by dispersing 10–20 mg of WO_3 powder in 50 mL of methanol. (A magnetic stirrer was used during the deposition to prevent settling.) The working electrode and counterelectrode were separated by 10 mm, and the voltage difference was 300 V. The EDP is based on the principle that oxide powders suspended in a liquid attain a surface charge. As a result, the charged particles move under the influence of an electric field and are deposited on an electrode. Since deposition always occurs at the anode, the WO_3 nanoparticles must attain a negative charge. An EDP duration of 1 min resulted in a film thickness of about 1 μm. It is interesting to note that WO_3 nanoparticle films could only be deposited when as-produced nanoparticles were substoichiometric (blue powder). When stoichiometric tungsten oxides (yellow powder) were used, films were not obtained. The blue EDP-deposited nanoparticle films became transparent after annealing in air at 300 °C for 2 h. Amorphous WO_3 films were prepared by conventional thermal evaporation of WO_3 (99.99 % purity). The thickness of the sample was about 1 μm. The crystalline films were prepared by heat-treating amorphous films at 400 °C in air for 2 h.

Cyclic voltammetry in a 1 M H_2SO_4 electrolyte solution was employed for the electrochemical characterization, and measurements were performed at room temperature between +1.0 and –0.1 V at various scan rates. Pt foil was used as the counter electrode and Ag/AgCl as the reference electrode. For CE measurements, the same quantity of protons was inserted for each sample while maintaining a constant current. In situ transmittance was measured using a laser diode at 670 nm, and was recorded as a function of time by using a computer-controlled potentiostat. TEM was performed on a Phillips CM-30 transmission electron microscope operating at 200 kV with a 50 μm objective aperture. The XRD diffractometer used was a Scintag PTS 4-circle goniometer with a Cu target operated at 45 kV and 36 mA (~1.6 kW) and a LN_2-cooled Ge detector. Sample preparation has been described previously by Mahan et al. [25]. SEM analysis was performed on a JEOL 6320 field-emission scanning electron microscope [27].

Received: September 14, 2005
Final version: January 9, 2006

[1] C. M. Lampert, *Sol. Energy Mater. Sol. Cells* **2003**, *76*, 489.
[2] C. M. Lampert, *Glass Sci. Technol.* **2002**, *75*, 244.
[3] M. Green, K. Pita, *Sol. Energy Mater. Sol. Cells* **1996**, *43*, 393.
[4] S.-H. Lee, H. M. Cheong, P. Liu, D. Smith, C. E. Tracy, J. R. Pitts, S. K. Deb, *J. Appl. Phys.* **2000**, *88*, 3076.
[5] S. K. Deb, *Philos. Mag.* **1973**, *27*, 801.
[6] C. G. Granqvist, *Handbook of Inorganic Electrochromic Materials*, Elsevier, New York **1995**.
[7] C. Bechinger, S. Ferrere, A. Zaban, J. Sprague, B. A. Gregg, *Nature* **1996**, *383*, 608.
[8] S.-H. Lee, H. M. Cheong, J.-G. Zhang, A. Mascarenhas, D. K. Benson, S. K. Deb, *Appl. Phys. Lett.* **1999**, *74*, 242.
[9] M. Grätzel, *Nature* **2001**, *409*, 575.
[10] M. Wagemaker, A. P. M. Kentgens, F. M. Mulder, *Nature* **2002**, *418*, 397.
[11] S.-H. Lee, H. M. Cheong, C. E. Tracy, A. Mascarenhas, J. R. Pitts, G. Jorgensen, S. K. Deb, *Appl. Phys. Lett.* **2000**, *76*, 3908.
[12] S.-H. Lee, H. M. Cheong, C. E. Tracy, A. Mascarenhas, A. W. Czanderna, S. K. Deb, *Appl. Phys. Lett.* **1999**, *75*, 1541.
[13] P. Chandrasekhar, B. J. Zay, G. C. Birur, S. Rawal, E. A. Pierson, L. Kauder, T. Swanson, *Adv. Funct. Mater.* **2002**, *14*, 3118.
[14] F. Fungo, S. A. Jenekhe, A. J. Bard, *Chem. Mater.* **2003**, *15*, 1264.
[15] A. A. Argun, A. Cirpan, J. R. Reynolds, *Adv. Mater.* **2003**, *15*, 1338.
[16] P. D. Yang, D. Y. Zhao, D. I. Margolese, B. F. Chmelka, G. D. Stucky, *Chem. Mater.* **1999**, *11*, 2813.
[17] S.-H. Lee, M. J. Seong, H. M. Cheong, C. E. Tracy, S. K. Deb, *Solid State Ionics* **2003**, *156*, 447.
[18] J.-P. Randin, *J. Electron. Mater.* **1978**, *7*, 47.
[19] B. W. Faughnan, R. S. Crandall, in *Topics in Applied Physics*, Vol. 40 (Eds: C. E. Acheron, H. J. Koelsch) Springer, Heidelberg, Germany **1980**, pp. 181–211.
[20] S. H. Baeck, T. Jaramillo, G. D. Stucky, E. W. McFarland, *Nano Lett.* **2002**, *2*, 831.
[21] S. S. Sun, P. H. Holloway, *J. Vac. Sci. Technol., A* **1984**, *A2*, 336.
[22] C. Bechinger, M. S. Burdis, J.-G. Zhang, *Solid State Commun.* **1997**, *101*, 753.
[23] A. Temmink, O. Anderson, K. Bange, H. Hantsche, X. Yu, *Thin Solid Films* **1990**, *192*, 211.
[24] E. Ozkan, S.-H. Lee, C. E. Tracy, F. Z. Tepehan, J. R. Pitts, S. K. Deb, *Sol. Energy Mater. Sol. Cells* **2003**, *79*, 439.
[25] A. H. Mahan, P. A. Parilla, K. M. Jones, A. C. Dillon, *Chem. Phys. Lett.* **2005**, *413*, 88.
[26] A. C. Dillon, A. H. Mahan, P. A. Parilla, J. L. Alleman, M. J. Heben, K. M. Jones, K. E. H. Gilbert, *Nano Lett.* **2003**, *3*, 1425.
[27] A. C. Dillon, A. H Mahan, R. Deshpande, C. Engtrakul, J. L. Alleman, J. L. Blackburn, K. E. H. Gilbert, M. J. Heben, P. A. Parillia, K. M. Jones, R. To, S-H. Lee, J. H. Lehman, *Thin Solid Films* **2006**, *501*, 216.

